LANGMUIR

pubs.acs.org/Langmuir Article

Protein Ligand-Induced Amplification in the 1/*f* Noise of a Protein-Selective Nanopore

Jiaxin Sun, Avinash Kumar Thakur, and Liviu Movileanu*

Cite This: *Langmuir* 2020, 36, 15247−15257 Read Online

ACCESS | Metrics & More | Article Recommendations | Supporting Information

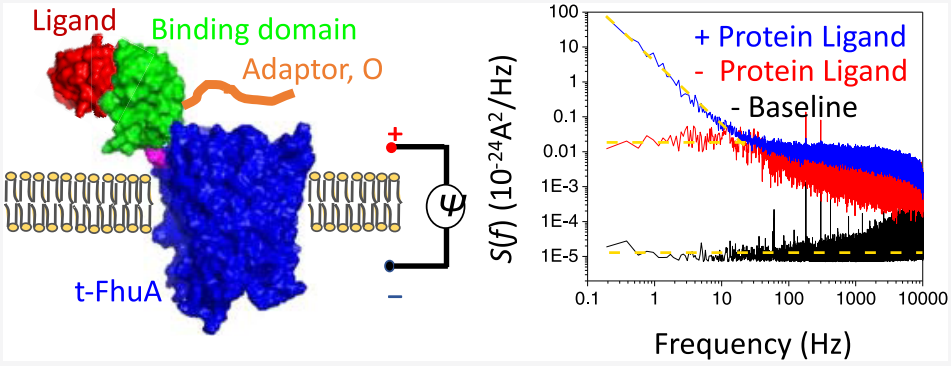

ABSTRACT: Previous studies of transmembrane protein channels have employed noise analysis to examine their statistical current fluctuations. In general, these explorations determined a substrate-induced amplification in the Gaussian white noise of these systems at a low-frequency regime. This outcome implies a lack of slowly appearing fluctuations in the number and local mobility of diffusing charges in the presence of channel substrates. Such parameters are among the key factors in generating a low-frequency 1/*f* noise. Here, we show that a protein-selective biological nanopore exhibits a substrate-induced amplification in the 1/*f* noise. The modular composition of this biological nanopore includes a hydrophilic transmembrane protein pore fused to a water-soluble binding protein on its extramembranous side. In addition, this protein nanopore shows an open substate populated by a high-frequency current noise because of the flickering of an engineered polypeptide adaptor at the tip of the pore. However, the physical association of the protein ligand with the binding domain reversibly switches the protein nanopore from a high-frequency noise substate into a quiet substate. In the absence of the protein ligand, our nanopore shows a low-frequency white noise. Remarkably, in the presence of the protein ligand, an amplified low-frequency 1/*f* noise was detected in a ligand concentration-dependent fashion. This finding suggests slowly occurring equilibrium fluctuations in the density and local mobility of charge carriers under these conditions. Furthermore, we report that the excess in 1/*f* noise is generated by reversible switches between the noisy ligand-released substate and the quiet ligand-captured substate. Finally, quantitative aspects of the low-frequency 1/*f* noise are in accord with theoretical predictions of the current noise analysis of protein channel−ligand interactions.

INTRODUCTION

β-Barrel protein pores, porins, and channels represent key permeation mechanisms across outer membranes of Gram-negative bacteria, mitochondria, and chloroplasts.[1,2] In addition, toxins secreted by various pathogens form *β*-barrel pores that induce cell lysis once inserted into a target membrane.[3,4] Standard single-channel analysis of the time domain in the form of time-resolved events identified that these proteins exhibit current transitions among various substates, spanning a broad range of durations. However, using the analysis of the frequency domain through a fast Fourier transformation (FFT) approach, the power spectral density (PSD) of these proteins revealed the amplitude distribution of the statistical current fluctuations measured at various frequencies. Wohnsland and Benz (1997)[5] have previously documented that the open state of many bacterial *β*-barrel porins exhibits 1/*f* noise in the low-frequency regime (0−100 Hz) or the so-called flicker noise.[6,7] 1/*f* noise is generated by slowly occurring equilibrium fluctuations in the number and local diffusion of charge carriers.[7,8] Previous studies have demonstrated that 1/*f* flicker noise is ubiquitous in protein pores,[9,10] porins,[11−14] and channels,[15,16] as well as in other ion-conduction synthetic systems, such as solid-state nanopores.[10,17−26] However, some *β*-barrel proteins[27−30]

Received: August 23, 2020
Revised: November 26, 2020
Published: December 13, 2020

https://dx.doi.org/10.1021/acs.langmuir.0c02498
Langmuir 2020, 36, 15247−15257

showed a frequency-independent Gaussian white noise in a broader frequency range, including the low-frequency regime. The absence of the frequency-dependent $1/f$ noise at low frequencies indicates the lack of significant equilibrium fluctuations in the density and local mobility of charge carriers across these β-barrels. Very recently, Dekker and co-workers (2020) have reviewed the comparisons and contrasts of different aspects of current noise in biological and synthetic nanopores.[10]

In general, two distinct protein systems have been previously observed with respect to substrate-induced modulation of the excess spectral noise. First, there are protein pores, porins, and channels, such as staphylococcal α-hemolysin[27−30] and outer-membrane protein F (OmpF)[31,32] of *Escherichia coli*, which exhibited a flat "white noise" in the low-frequency regime in the absence of any chemical agent. However, the presence of a small-molecule ligand at concentrations near half of the equilibrium dissociation constant, K_d, produced an excess in the white noise of these protein systems. Second, there are other protein systems, such as the protective antigen (PA63) channel of the anthrax toxin[33,34] and maltoporins,[11−14,35−37] which showed a $1/f$ flicker noise in the low-frequency domain. However, the addition of a small-molecule ligand or a channel blocker ignited an excess in the white noise in this low-frequency range.[11−14,33−37] Therefore, these prior studies indicated that the small-molecule ligands significantly increase the white noise in the low-frequency domain.

In this paper, we provide compelling experimental evidence that a protein-selective β-barrel protein nanopore shows a protein ligand-induced amplification in the frequency-dependent $1/f$ noise. The functional architecture and modular composition of this protein nanopore are inspired by the structure−function properties of outer-membrane proteins of Gram-negative bacteria. Specifically, its transmembrane stem is the β-barrel of ferric hydroxamate uptake component A (FhuA)[38,39] of *E. coli*. This is a 455-residue single-polypeptide protein, also called t-FhuA (Figure 1a).[40] The binding domain of the nanopore is a 110-residue, water-soluble RNAse barnase (Bn),[41] which cannot fit within the hydrophilic pore interior. Therefore, Bn was tethered outside the t-FhuA pore at its N-terminus through a flexible Gly/Ser-based hexapeptide. This was the basis for generating a synthetic Bn-t-FhuA nanopore (Experimental Section).[40] Barstar (Bs),[42] the high-affinity 89-residue inhibitor for Bn, was employed as a protein ligand.[43] Previously, the Bn−Bs complex formation has been readily observed at single-recognition event precision in homogeneous solutions[40] and in heterogeneous biological fluids.[44] These explorations were facilitated by the presence of a dodecapeptide adaptor (O), which was engineered at the N-terminus of Bn.

Here, we analyze these Bn−Bs interactions at a very broad bandwidth and show that Bn-t-FhuA exhibits an open substate of high-frequency current noise in the absence of Bs. This high-frequency current noise is likely due to frequent and short-lived moieties of the adaptor, O, at the tip of the t-FhuA pore (Figure 1b). In contrast, our protein-selective biological nanopore lies in a quiet substate when Bs is transiently captured by the Bn binding domain. In the latter case, the O adaptor is likely detached from the pore opening. Reversible Bn−Bs complex formations within the extramembranous side of t-FhuA can be observed through stochastic alternations of the quiet substates and high-frequency noise events. Furthermore, when Bs was not present in solution, a uniform

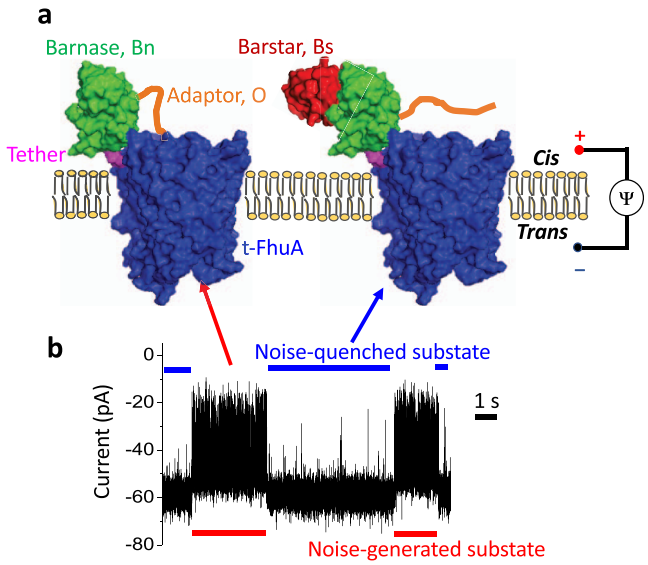

Figure 1. Composition of Bn-t-FhuA, a protein-selective protein nanopore. (a) This single-polypeptide protein nanopore comprises a heavily truncated ferric hydroxamate uptake protein A of *E. coli* (t-FhuA), which is marked in blue.[48] This truncated β-barrel outer-membrane protein pore, which serves as the transmembrane permeation pathway of ions, was fused at its N-terminus to a Bn (marked in green) protein via a flexible Gly/Ser-based hexapeptide tether (marked in magenta).[40] An unstructured dodecapeptide adaptor (O, marked in orange) at the N-terminus of Bn flickered at the tip of the pore opening. (b) Snapshot of a single-channel electrical trace of Bn-t-FhuA when Bs (marked in red) was added to the *cis* side of the chamber. Bs produced stochastic conductance switches between high-frequency current noise-generated substates and high-frequency current noise-quenched substates.

and voltage-dependent current noise of Bn-t-FhuA, which is reminiscent of a flat ("white") noise, was noted in the low-frequency regime.

In this article, we provide experimental substantiation that the reversible switches of the Bs-captured and Bs-released substates produce a significant amplification in the frequency-dependent $1/f$ flicker noise.[5] The maximum of the low-frequency $1/f$ noise amplification is reached at a Bs concentration near $K_d/2$, where K_d is the equilibrium dissociation constant. This experimental outcome is in accordance with theoretical predictions of the current noise analysis of ligand-gated ion channels. Remarkably, the presence of Bs at concentrations much greater than the K_d value abolished the amplification in the $1/f$ noise and reverted the signature of current noise of Bn-t-FhuA to a white-noise pattern in the low-frequency domain.

EXPERIMENTAL SECTION

Cloning and Mutagenesis of the Protein Nanopore and Protein Ligand. Conventional and assembly PCR techniques were employed to create all genes used in this work. Cloning was conducted using the pPR-IBA1 expression vector. The primary gene, *obn(ggs)$_2$t-fhua*, encoded the Bn-t-FhuA nanopore, which included the dodecapeptide adaptor (MGDRGPEFELGT), fused at the N-terminus of Bn, a flexible glycine/serine-rich hexapeptide arm (GGSGGS), as well as an extensively truncated ferric hydroxamate uptake protein A (t-FhuA) and *KpnI* sites at both ends.[40,44] This gene was developed using genes of individual Bn and t-FhuA proteins, *bn* and *t-fhua*, respectively, and assembly PCR reactions. An H102A mutant of Bn was used because this suppressed RNase activity so that

https://dx.doi.org/10.1021/acs.langmuir.0c02498
Langmuir 2020, 36, 15247−15257

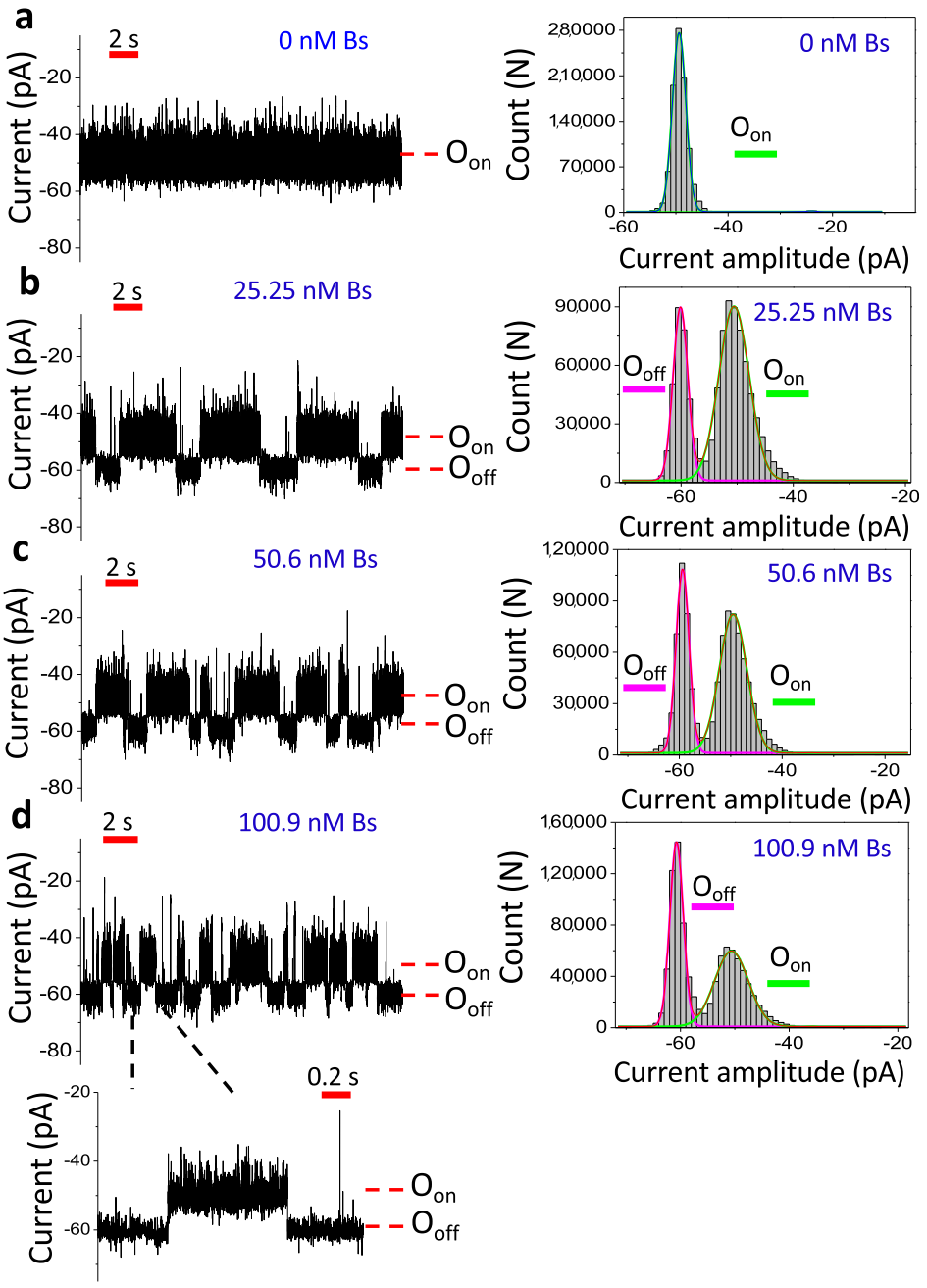

Figure 2. High-bandwidth single-channel data acquisitions of Bn-t-FhuA in the presence of Bs. Single-channel electrical traces, which were filtered at 1 kHz using a low-pass eight-pole Butterworth filter, are provided for Bs concentrations of 0 (a), 25.25 (b), 50.6 (c), and 100.9 nM (d) added to the *cis* side of the chamber. The O_{on} and O_{off} levels represent the Bs-released and Bs-captured substates. The applied transmembrane potential was −40 mV. The inset in (d) is an example of the Bs-released substate event. For the sake of clarity, this single-channel electrical trace was also filtered at 1 kHz using a low-pass eight-pole Butterworth filter. The corresponding all-point current amplitude histograms are displayed on the right side. Maxima of the peaks of the current amplitude represent substate "off" (Bs-captured event, O_{off}, left) and open substate "on" (Bs-released event, O_{on}, right). The following values are provided as the mean ± standard error of the mean (s.e.m). (a) O_{on} was −49.4 ± 0.1 pA. (b) O_{on} and O_{off} were −50.6 ± 0.1 pA and −60.1 ± 0.1 pA, respectively. (c) O_{on} and O_{off} were −49.5 ± 0.1 and −59.4 ± 0.1 pA, respectively. (d) O_{on} and O_{off} were −50.6 ± 0.1 and −60.7 ± 0.1 pA, respectively. All-point current amplitude histograms were developed using 20 s duration single-channel electrical traces. The bin size of these histograms is 1 pA. These single-channel electrical traces are representative over a subset of at least n = 3 distinct experiments.

Bn-t-FhuA is not toxic to the expression host.[41,45] In addition, the *bs* gene of Bs included a double-alanine mutant, C40A/C82A.[46]

Protein Expression, Purification, and Refolding. Protocols for protein expression and purification of the Bn-t-FhuA nanopore were previously reported.[47,48] Lyophilized Bn-t-FhuA samples were solubilized in 200 mM KCl, 8 M urea, 50 mM Tris−HCl, pH 8 to a concentration of ∼15 μM and then placed at room temperature for several hours. Refolding of the denatured Bn-t-FhuA samples was accomplished by adding n-dodecyl-β-D-maltopyranoside (DDM) to a final concentration of 1.5% (w/v).[49,50] Then, a slow dialysis of protein samples was conducted against 200 mM KCl, 20 mM Tris−HCl, pH 8 at 4 °C for at least 3 days. Bn-t-FhuA samples for single-channel electrical recordings were obtained by 20-fold dilution in 200 mM KCl, 20 mM Tris−HCl, pH 8, 0.5% DDM. For the Bs protein,

https://dx.doi.org/10.1021/acs.langmuir.0c02498
Langmuir 2020, 36, 15247−15257

transformed cells were grown in the Luria−Bertani medium at 37 °C until OD_{600} was ∼0.5. Then, the temperature was reduced to 20 °C, and induction was performed in the presence of isopropyl β-d-1-thiogalactopyranoside.[40] The cells were further cultured for a period of ∼18 h using the same temperature. Cultured cells were centrifuged at 3700*g* at 4 °C for 30 min and then resuspended in 150 mM KCl, 50 mM Tris−HCl, 5 mM EDTA, pH 8. This step was followed by cell lysis using a model 110L microfluidizer (Microfluidics, Newton, MA). The supernatant and insoluble pellet were separated by centrifuging the lysates at 108,500*g* at 4 °C for 30 min. Then, the supernatant, which was processed through ammonium sulfate precipitation, was dialyzed overnight at 4 °C against 20 mM Tris−HCl, pH 8 and purified on a Q-Sepharose column (Bio-Rad, Hercules, CA). A further purification step was performed using size exclusion chromatography (SEC) via a Superdex-75 size-exclusion column (GE Healthcare Life Sciences, Pittsburg, PA).

Current Noise and Single-Channel Electrical Recordings Using Planar Lipid Bilayers. Standard protocols for single-channel electrical recordings were employed using planar lipid membranes.[51,52] The Bn-t-FhuA nanopore was added to the *cis* side of the chamber (Figure 1a) at a final concentration in the range of 0.3−1 ng/μL. The *cis* side was grounded, implying that an applied positive potential corresponds to the translocation of positive ions from the *trans* to *cis* side of the chamber. The electrolyte solution contained 300 mM KCl, 10 mM Tris−HCl, pH 8. All recordings were obtained at room temperature (23 ± 1 °C). Single-channel electrical currents were obtained using an Axopatch 200B patch-clamp amplifier (Axon Instruments, Foster City, CA). Electrical signals were digitized using a low-noise acquisition system, model Axon 1440A (Axon Instruments), sampled at a frequency of 50 kHz, and filtered at a filter frequency of 10 kHz using a low-pass eight-pole Butterworth filter, model 900B (Frequency Devices, Ottawa, IL), unless otherwise stated. Single-channel electrical data acquisition and analysis were executed using the pClamp 10.5 software package (Axon) and Origin 8.5 (OriginLab, Northampton, MA).

The PSD was generated in ClampFit (pClamp, Axon) by using a built-in power spectrum function applied to single-channel electrical traces. In this way, an FFT method was digitally employed. The low-frequency limit of PSD, $S(0)$, was determined from the lowest experimental frequency of the PSD of current noise. For the relationship $S(0) \propto (\Delta I)^2$, where ΔI is the absolute difference in the single-channel electrical currents between the Bs-released and Bs-captured substates, the average values of these currents were determined from Gaussian fits of all-point histograms of these two open substates. Fits of $1/f^{\varepsilon}$ flicker noise in the low-frequency domain of the PSD were conducted in a log−log representation and in the frequency range of (f_{min}, f_{cut}), where f_{min} and f_{cut} are the minimum experimental frequency in the PSD and the cutoff frequency, respectively. Here, f_{cut} is the experimental frequency that corresponds to the onset of the low-frequency $1/f$ flicker noise. Fits of white noise in the low-frequency domain of the PSD were conducted using a Lorentzian function

$$S(f) = \frac{S(0)}{1 + \left(\frac{f}{f_c}\right)^2} \quad (1)$$

where f_c is the corner frequency. Filter frequencies of either 100 Hz or 1 kHz were also used for data analysis of the low-frequency domain (f_{min}—100 Hz) as they do not affect the PSD of this spectrum range. In general, 15 individual 10 s duration single-channel electrical traces, which were filtered at a frequency of 10 kHz using a low-pass eight-pole Butterworth filter, were used to obtain average values of low-frequency noise parameters $S(0)$ and f_c[34,53] unless otherwise stated. Shorter-duration electrical traces were also employed to analyze individual Bs-released or Bs-captured substates.

RESULTS AND DISCUSSION

Single-Channel Electrical Signature of a Protein-Selective Protein Nanopore. Our single-polypeptide chain protein nanopore, Bn-t-FhuA, consists of the t-FhuA pore,[40] an extensive truncation of the outer-membrane protein FhuA[38,39] of *E. coli*, which was fused to Bn, a small RNase Bn (Figure 1a).[41] The fusion of both proteins was conducted at the N-terminus of t-FhuA via a flexible Gly−Ser hexapeptide tether. This construct also included the O adaptor, a dodecapeptide extension fused at the untethered terminus of Bn (Experimental Section). This dodecapeptide is slightly negatively charged and unstructured in solution.[54] The O adaptor should cover the distance between the entrance of t-FhuA and the untethered terminus of Bn. A representative single-channel signature of our protein-selective nanopore, Bn-t-FhuA, is shown in Figure 2a. At a transmembrane potential of −40 mV and in 300 mM KCl, 10 mM Tris−HCl, pH 8.0, this signature corresponds to an open-channel conductance, g_{open}, of 1.26 ± 0.02 nS (n = 3). g_{open} was determined using the average current corresponding to the peak maximum resulting from an all-point current amplitude histogram (Figure 2a). This open substate (O_{on}) was populated by highly frequent and short-lived current spikes. Many current spikes were not time-resolvable, so they lacked well-defined current levels. Remarkably, the addition of 25.25 nM Bs[42] to the *cis* side of the chamber produced reversible switches between substates containing current spikes and substates free of current spikes (Figure 2b, Supporting Information, Figure S1). In the absence of the O adaptor, these Bn−Bs binding events were not noted in the current recordings because these interactions occurred outside the t-FhuA nanopore.[40] Thus, the O adaptor produced distinctive current levels of the high-frequency noise-generated open substate (O_{on}) and the high-frequency noise-quenched open substate (O_{off}). For example, this resulted in shifting the high-frequency noise-generated open substate (O_{on}) to the high-frequency noise-quenched open substate (O_{off}), whose conductance, g^*_{open}, was increased to 1.52 ± 0.02 nS ($g^*_{open} > g_{open}$, n = 3) (Figure 2b). g^*_{open} was also calculated using the average current of the corresponding peak maximum, which resulted from an all-point current amplitude histogram.

The frequency of the high-frequency noise-quenched open substate events (O_{off}) was elevated at increased Bs concentrations (Figure 2cd; Supporting Information, Figure S1), leading to reduced durations of the high-frequency noise-generated substate events (O_{on}). Here, let us denote by τ_{on} and τ_{off} the average durations of the high-frequency noise-generated open substate (O_{on}) and the high-frequency noise-quenched open substate (O_{off}), respectively. Previously, we demonstrated that a change in $1/\tau_{on}$ scaled in a ratio of 1:1 with a change in the Bs concentration, whereas τ_{off} was independent of the Bs concentration.[40,44] This result was obtained at a highly increased signal filtering so that these events were unambiguously determined through their current amplitudes as the occurrence and suppression of the short-lived current spikes coincide with the current levels of the O_{on} and O_{off} events, respectively. Therefore, the O_{on} (corresponding to g_{open}) and O_{off} (corresponding to g^*_{open}) substates represent the Bs-released and Bs-captured events, respectively. In this way, $k_{on} = 1/([Bs]\tau_{on})$ and $k_{off} = 1/\tau_{off}$ are the association and dissociation rate constants, respectively, where [Bs] is the Bs concentration. In other words, the Bs-captured and Bs-released events occurred as bimolecular association and unimolecular dissociation processes, respectively. Interestingly, the unitary conductance of the quiet open substate of Bn-t-FhuA (O_{off}) was closely similar to those values recorded with an O adaptor-free Bn-t-FhuA pore or with a t-FhuA pore

https://dx.doi.org/10.1021/acs.langmuir.0c02498
Langmuir 2020, 36, 15247−15257

($g_{t\text{-}FhuA}$ = 1.6 ± 0.1 pS),[40] suggesting that Bn was indeed exclusively located on the extramembranous side of the nanopore.

What Is the Role Played by the O Adaptor? To produce a detectable signal of the Bs-capture and Bs-release events, additional development of this protein sensor was necessary. The dodecapeptide O adaptor, which was engineered at the N-terminus of the Bn binding domain, signals the physical associations and dissociations of Bs with Bn in real time. Without the O adaptor, Bn-t-FhuA exhibits a larger-conductance open substate (~1.52 nS) that is relatively quiet.[40] However, with the engineered O adaptor, Bn-t-FhuA shows a lower-conductance open substate (~1.26 nS) that is very noisy. Thus, the O adaptor not only produced a slightly lower conductance of the Bn-t-FhuA nanopore with respect to that of t-FhuA but also created highly frequent and short-lived current spikes. Here, we tentatively interpret that a reduced transmembrane current and short-lived current spikes of the O_{on} substate result from the interactions of the slightly negatively charged O adaptor with the positively charged groups located on the nanopore entrance. The Bs-captured event, which was identified by the O_{off} substate, is accompanied by the detachment of the O peptide from the pore opening, thus increasing and quieting the transmembrane current. A comprehensive understanding of these conformational changes as well as their coordination with the single-channel current fluctuations might be accomplished by full-atomistic molecular dynamics (MD) simulations of the entire biomolecular system[55] and under similar experimental conditions. Insightful information from these MD simulations might prove instrumental for the extension of this approach to other protein ligand−protein receptor pair interactions.

Bs-Amplified 1/*f* Noise of the Bn-t-FhuA Nanopore. Throughout this article, experimental values of the low-frequency limit, $S(0)$, are the current noise amplitudes that correspond to the lowest measured frequency in the PSD. In the absence of Bs and at a zero transmembrane potential, we observed a flat ("white") noise of Bn-t-FhuA with $S(0)$ in the range of $(2 - 6) \times 10^{-29}$ A^2/Hz (Figure 3a; Supporting Information, Figures S2−S7). These values were near the sum of the Johnson−Nyquist thermal noise[12,25,56−60] of 2.06×10^{-29} A^2/Hz and the shot noise[12,25,58−60] of 1.61×10^{-29} A^2/Hz (Supporting Information, Supporting Methods)[25,61]

$$S_{white} = S_{thermal} + S_{shot} \quad (2)$$

These values were obtained using the single-channel conductance of ~1.26 nS for Bn-t-FhuA (Figure 2a). This white-noise signature was also noted at both negative and positive transmembrane potentials (Supporting Information, Figures S4−S7, Table S1). The Bs-free and Bs-amplified $S(0)$ were proportional to either the square of transmembrane potential or the square of transmembrane current (Supporting Information, Figures S8 and S9, Table S2). Therefore, $S(0)$ corresponds to a quadratic function that depends on the applied transmembrane potential, a situation also found with other porins[14] or other solid-state systems.[6,62]

Remarkably, at a transmembrane potential of −40 mV, the presence of 25.25 nM Bs drastically enhanced the low-frequency limit of the PSD of current noise, $S(0)$, almost 4 orders of magnitude with respect to the background current noise in the absence of Bs (Figure 3a). Moreover, the profile of the Bs-amplified current noise is reminiscent of low-frequency 1/*f* flicker noise, which had an onset at a cutoff frequency, f_{cut}, of ~40 Hz. However, Bs-dependent $S(0)$ followed a biphasic dependence on the Bs concentration (Figure 3b; Supporting Information, Figures S10−S15). For example, $S(0)$ increased from $(12.2 \pm 0.6) \times 10^{-27}$ A^2/Hz in a Bs-free solution (Supporting Information, Table S2) to $(42.9 \pm 5.6) \times 10^{-24}$ A^2/Hz and $(71.1 \pm 9.7) \times 10^{-24}$ A^2/Hz at Bs concentrations of 12.63 and 25.25 nM, respectively (Supporting Information, Table S3). Then, $S(0)$ gradually decreased at Bs concentrations greater than 25.25 nM. The biphasic pattern of $S(0)$ with respect to the substrate concentration was also discovered when small-molecule analytes interacted with binding sites within protein pores.[27,28,36,63] In this work, the maximum of the low-frequency limit of excess 1/*f* noise was reached at a Bs concentration near half of the K_d. This outcome agrees well with previous theoretical estimates of the dependence of $S(0)$ on the substrate concentration.[27,64]

The current dependence of $S(0)$ is given by the following formula[64]

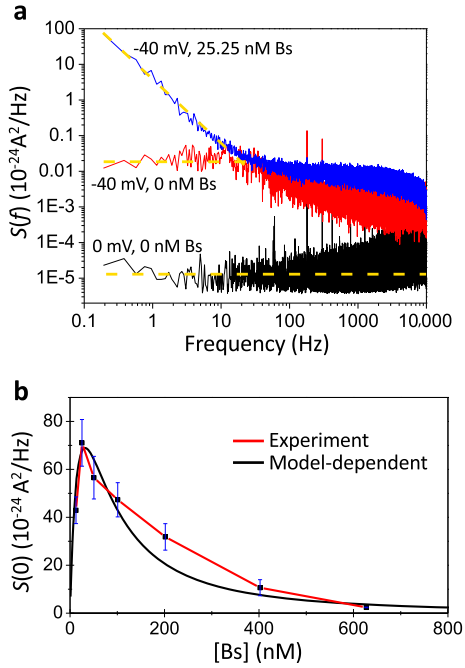

Figure 3. Excess spectral density of current noise of the Bn-t-FhuA nanopore as a function of the Bs ligand concentration and at a negative transmembrane potential. $S(f)$ was obtained from a 10 s duration single-channel electrical trace. Each trace included both the Bs-released and Bs-captured substates. Single-channel electrical traces were filtered at 10 kHz using a low-pass eight-pole Butterworth filter. (a) Representative PSD of current noise of the Bn-t-FhuA nanopore in a log−log representation. The PSD was averaged over n = 15 different PDSs obtained from distinct single-channel electrical traces. Data were recorded at 0 mV without Bs (black), at −40 mV without Bs (red), and at −40 mV in the presence of 25.25 nM Bs (navy). (b) Linear-scale plot that shows the comparison of model-dependent $S(0)$ with experimental $S(0)$, which was recorded from the PSD of current noise, vs the Bs concentration. The low-frequency limit of the excess spectral density, $S(0)$, was obtained as the average over 15 distinct 10 s duration single-channel electrical traces recorded from n = 3 distinct experiments at a transmembrane potential of −40 mV. Data points represent the mean ± standard deviation (s.d.) obtained from n = 3 distinct experiments.

https://dx.doi.org/10.1021/acs.langmuir.0c02498
Langmuir 2020, 36, 15247−15257

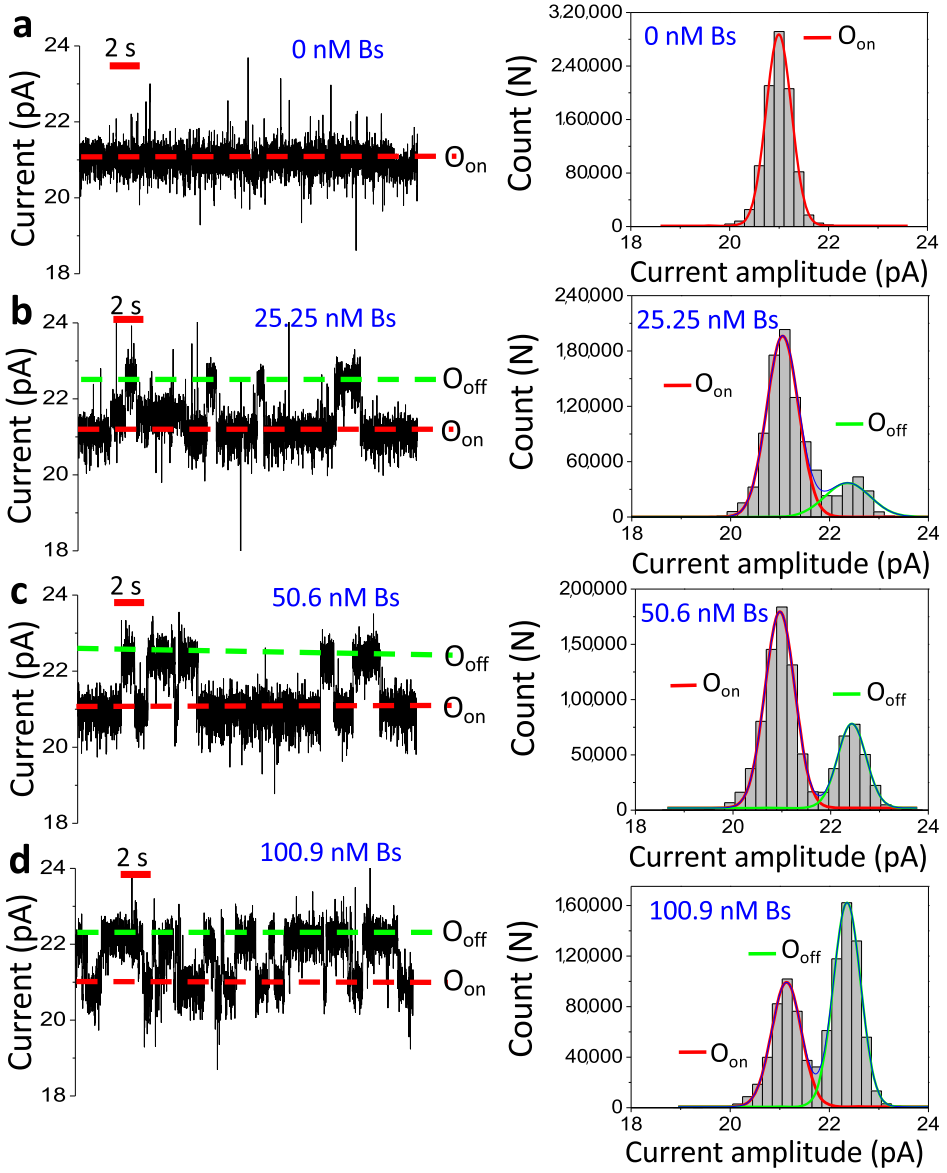

Figure 4. High-bandwidth single-channel electrical recordings of Bn-t-FhuA in the presence of Bs at a positive potential. Single-channel electrical traces, which were filtered at 100 Hz using a low-pass eight-pole Butterworth filter, are provided for Bs ligand concentrations of 0 (a), 25.25 (b), 50.6 (c), and 100.9 nM (d) added to the *cis* side of the chamber. The O_{on} and O_{off} levels represent the Bs ligand-released and Bs ligand-captured open substates. The applied transmembrane potential was +15 mV. The following values are provided as the mean ± s.e.m. (a) O_{on} was 21.0 ± 0.1 pA. (b) O_{on} and O_{off} were 21.1 ± 0.1 and 22.4 ± 0.1 pA, respectively. (c) O_{on} and O_{off} were 20.9 ± 0.1 and 22.4 ± 0.1 pA, respectively. (d) O_{on} and O_{off} were 21.1 ± 0.1 and 22.4 ± 0.1 pA, respectively. The corresponding all-point current amplitude histograms are displayed on the right side. Multiple-peak Gaussian fittings were used. Maxima of the peaks of the current amplitude represent substates "off" (O_{off}, right) and "on" (O_{on}, left). The all-point current amplitude histograms were developed using 20 s duration single-channel electrical traces. The bin size of these histograms is 0.2 pA. These single-channel electrical traces are representative from a subset of at least n = 3 distinct experiments.

$$S(0) = 4(\Delta I)^2 \tau_{off} \frac{\frac{[L]}{K_d}}{\left(1 + \frac{[L]}{K_d}\right)^3} \tag{3}$$

where ΔI is the absolute difference in the transmembrane current between the Bs-captured and Bs-released substates. Here, [L] and K_d denote the Bs concentration and the equilibrium dissociation constant, respectively. τ_{off} is the binding duration, which is the reciprocal of the dissociation rate constant, k_{off}. Equation 3 exhibits a maximum value at a Bs concentration equal to one-half of the K_d

$$S(0) \rightarrow S(0)_{max} \qquad \text{when } [L] = \frac{K_d}{2} \tag{4}$$

In this case,

$$S(0)_{max} = \frac{16}{27}(\Delta I)^2 \tau_{off} \tag{5}$$

Therefore, $S(0)_{max}$ depends on the current difference between the two substates and the binding duration. Using the time-resolved analysis of current events with an absolute current difference between the Bs-captured and Bs-released substates, ΔI = 10 pA, the equilibrium dissociation constant, K_d = 64 nM, and the rate constant of dissociation, k_{off} = 0.86

https://dx.doi.org/10.1021/acs.langmuir.0c02498
Langmuir 2020, 36, 15247−15257

s^{-1},[40] we obtain a model-dependent $S(0)_{max}$ = 68.9 × 10^{-24} A^2/Hz, a value that is closely similar to that experimentally determined at a Bs concentration of 25.25 nM. Indeed, this Bs concentration is close to K_d/2, which is in accord with eq 4 (Figure 3b). This experimental finding is in good agreement with theoretical predictions of the low-frequency limit of the PSD (Supporting Information, Figures S16 and S17, Tables S3 and S4).[27,64]

What Is the Source of the Low-Frequency 1/*f* Flicker Noise? We then asked whether the dependence of $S(0)$ on the Bs concentration is reflected by the PSD of either the Bs-captured events or Bs-released events. A detailed analysis of these events illuminated that $S(0)$ of the Bs-released events was amplified by the presence of Bs in a biphasic signature (Supporting Information, Figures S18 and S19). This pattern was qualitatively similar to that noted in Figure 3b (Supporting Information, Figures S16 and S17). On the contrary, $S(0)$ of the Bs-captured events was reduced yet independent of the Bs concentration in the range of 12.63−627.3 nM (Supporting Information, Figures S20−S22). Therefore, the presence of the Bs has an opposite effect on the substates of the Bn-t-FhuA nanopore, increasing $S(0)$ of the Bs-released events but decreasing $S(0)$ of the Bs-captured events. Enhancing the Bs concentration shortens the total duration of the Bs-released substate and lengthens the total duration of the Bs-captured substate. Hence, we postulate that the Bs concentrations in excess would normally lead to a significant reduction in the current noise (see below). Furthermore, the Bs-released substate and the Bs-captured substate are virtually 1/*f* noise-free in the low-frequency domain (Supporting Information, Figures S20 and S21). This outcome suggests that the discrete current switches between the Bs-captured and Bs-released substates (Figures 1 and 2) contribute at least in part to the generation of low-frequency 1/*f* flicker noise.[12]

Is the Low-Frequency Limit of the 1/*f* Noise Biphasic at a Positive Potential As Well? We then asked whether the Bs-amplified 1/*f* current noise, which was noted in a biphasic pattern with respect to the Bs concentration, can also be obtained at a positive potential. If so, are the experimental $S(0)$ values in accordance with theoretical predictions of the current noise analysis? Therefore, we examined the spectral noise both quantitatively and qualitatively at a positive transmembrane potential. Single-channel electrical recordings in the presence of low-nanomolar Bs concentrations at a transmembrane potential of +15 mV are illustrated in Figure 4. In the absence of Bs, the unitary conductance, g_{open}, of Bn-t-FhuA was 1.42 ± 0.01 nS (O_{on}; Bs-released substate; Figure 4a). However, in the presence of Bs, transient openings of Bn-t-FhuA to an O_{off} substate of conductance, g^*_{open}, of 1.48 ± 0.02 nS ($g^*_{open} > g_{open}$, n = 3, Bs-captured substate; Figure 4b) occurred in a concentration-dependent fashion (Figure 4bcd; Supporting Information, Figure S23). Interestingly, under similar experimental conditions, the absolute current difference between the O_{on} and O_{off} substates, ΔI, was ∼1.2 pA at +15 mV, a value significantly lower than that obtained at −40 mV (∼10 pA). These current difference values correspond to conductance difference values, Δg, of ∼0.08 and 0.25 nS, respectively.

Remarkably, the low-frequency domain also showed a 1/*f*-type noise signature (Figure 5a). Moreover, the Bs-induced excess in 1/*f* current noise depended on the Bs concentration in a biphasic fashion (Figure 5b), which is reminiscent of the outcomes resulting at a transmembrane potential of −40 mV. Here, $S(0)$ can also be calculated using eq 3 along with

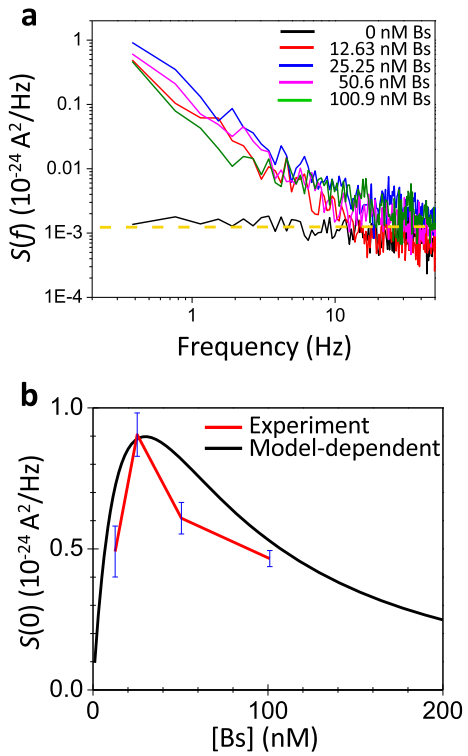

Figure 5. Excess spectral density of current noise of the Bn-t-FhuA nanopore as a function of the Bs ligand concentration and at a positive transmembrane potential. The low-frequency limit of the excess spectral density, $S(0)$, was obtained as a mean from 15 distinct 5 s duration single-channel electrical trace intervals recorded at a transmembrane potential of +15 mV. Each trace included both the Bs-released and Bs-captured substates. Single-channel electrical traces were further low-pass-filtered at 100 Hz using an eight-pole Butterworth filter. (a) Representative PSDs of current noise recorded at various Bs ligand concentrations. PSDs illustrated in (a) were averaged over n = 15 different PDSs obtained from n = 15 distinct single-channel electrical traces. (b) Comparison of model-dependent $S(0)$ with experimental $S(0)$ recorded from PSD from (a). Data points represent the mean ± s.d. obtained from n = 3 distinct experiments.

parameters derived from time-resolved analysis of discrete events. Using ΔI = 1.2 pA, K_d = 60 nM, and k_{off} = 0.95 s^{-1},[44] we obtain model-dependent $S(0)$ values, which are closely similar to experimentally determined $S(0)$ values (Figure 5b; Supporting Information, Figure S24, Table S5). The biphasic signature of $S(0)$ resulted, at least in part, from the alteration in the slope of 1/*f* current noise with respect to the Bs concentration. Hooge's phenomenological formula of the low-frequency 1/*f* current noise is[5,65−67]

$$S(f) = \frac{\alpha {I_0}^2}{N f^c} \tag{6}$$

where I_0 is the open-state single-channel current, N and f denote the number of channels in the membrane and frequency, respectively, and c is a constant. Here, α is Hooge's phenomenological parameter of current noise. We obtained values of α in the range of 0.001−0.002 at low-nanomolar Bs concentrations and at a transmembrane potential of −40 mV (Supporting Information, Table S3). However, these values were significantly lower, which were in the range of 0.0003−0.0005, at a transmembrane potential of +15 mV (Supporting

https://dx.doi.org/10.1021/acs.langmuir.0c02498
Langmuir 2020, 36, 15247−15257

Information, Table S5). Our Hooge's parameters are in accordance with those previously determined by other groups using various protein pore systems.[5,12]

Low-Frequency 1/*f*-Type Noise Signature Is Abolished at a High Occupancy of Bn. Next, we wanted to explore whether the Bs-induced $1/f$ noise is yet present at Bs concentrations much greater than the K_d under conditions of high occupancy of Bn-t-FhuA by Bs (Supporting Information, Figures S25−S28, Table S6). Thus, Bn-t-FhuA was exposed to low-micromolar Bs concentrations, which were in the range between a 20-fold increase and an 80-fold increase with respect to the K_d. In accordance with our expectation, $S(0)$ was drastically reduced in this range of Bs concentrations (Supporting Information, Figure S29). In addition, the very low-frequency regime (0.2 Hz < f < 30 Hz) of the PSD showed a rather white-noise signature (Supporting Information, Figures S30 and S31). This finding suggested that the Bs-amplified $1/f$ noise signature was nearly eliminated at Bs concentrations approaching the saturation of the Bn binding site. We observed that $S(0)$ recorded at Bs concentrations in excess gradually decreased by increasing the Bs concentration (Supporting Information, Table S7). For example, excess of Bs at a concentration of 4.8 μM, which is about ∼150-fold of the $K_d/2$, produced a significant, 530-fold reduction in the $1/f$ flicker noise with respect to its maximum value, $S(0)_{max}$. However, $S(0)$ was about 1 order of magnitude greater at 4.8 μM Bs than the value recorded in the absence of Bs under similar experimental conditions. This is a significantly reduced $S(0)$ value with respect to that obtained at 25.25 nM Bs (Figure 3a). Finally, the onset of the white-noise plateau in the form of a corner frequency, f_c,[14] increased at greater Bs concentrations (Supporting Information, Figure S32, Table S8).

Voltage Dependence of the Low-Frequency 1/*f* Flicker Noise. We also asked whether the $1/f$ flicker noise can be revealed at other transmembrane potentials than those presented above. Therefore, we have extensively explored the low-frequency domain at transmembrane potentials in the range of −50 mV through +50 mV (Supporting Information, Figures S33−S37). Figure 6a shows representative examples of the PSD of Bn-t-FhuA recorded at transmembrane potentials of ±5 and ±40 mV and in the presence of 12.63 nM Bs. These examples demonstrate that the low-frequency limit of the PSD increases by decreasing the frequency. In a log−log plot, linear fits of data for the low-frequency domain show a $1/f^c$ signature, where c is the power constant that was always greater than unity (Figure 6b; Supporting Information, Table S9). We also noted that the frequency onset of the $1/f^c$ signature of the PSD, f_{cut}, was voltage-dependent and slightly increased by enhancing the applied transmembrane potential in a U-shape fashion with respect to the voltage bias. Therefore, the $1/f$ noise signature is a conserved property regardless of the applied transmembrane potential. However, a greater transmembrane potential expands the range of the low-frequency domain that is subjected to this $1/f$ noise signature.

The lower $S(0)$ values at positive potentials with respect to negative voltage biases can be explained in terms of the lower absolute current difference, ΔI, between the Bs-captured and Bs-released substates. We employed Hooge's phenomenological formula (eq 6) for examining the characteristics of the Bs-amplified $1/f$ noise of the nanopore. However, we found that α, Hooge's phenomenological constant, was slightly greater at negative potentials (>0.001) than at positive potentials

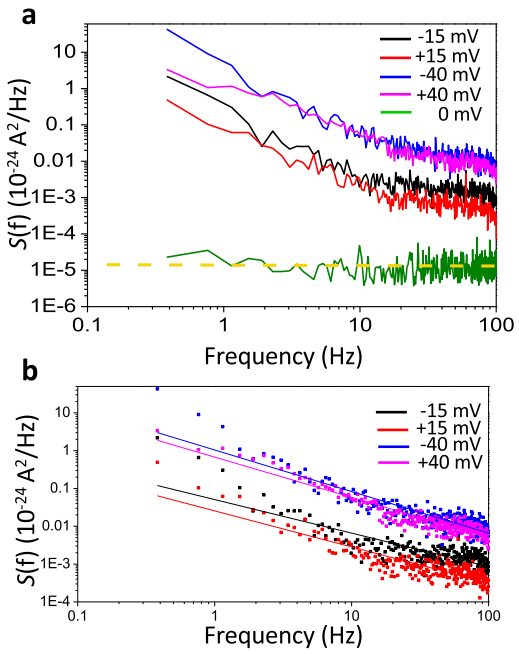

Figure 6. Low-frequency domain of the excess spectral density of current noise of the Bn-t-FhuA nanopore at various transmembrane potentials. $S(0)$ was obtained as the mean ± s.d. from 15 distinct 5 s duration traces recorded at 12.63 nM Bs. Each trace included both the Bs-released and Bs-captured substates. Single-channel electrical traces were further filtered at 100 Hz using a low-pass eight-pole Butterworth filter. (a) Representative averaged PSD of single-channel current noise recorded at various transmembrane potentials. PSDs illustrated in (a) were averaged over n = 15 different PDSs obtained from n = 15 distinct single-channel electrical traces. (b) Linear fits of the PSD data from (a) shown in a log−log representation.

(<0.001) (Supporting Information, Table S9), suggesting an asymmetry of the $1/f$ flicker noise with respect to the voltage bias. Therefore, $1/f$ flicker noise of the Bn-t-FhuA nanopore is characterized by a voltage asymmetry. This finding is not surprising given that t-FhuA shows a permeability ratio P_K/P_{Cl} of 5.5 ± 1.7 under the asymmetric conditions of 20 mM KCl/200 mM KCl.[68] Therefore, t-FhuA is a non-Ohmic transmembrane protein pore. The asymmetry of $1/f$ noise with respect to the voltage bias was also discovered in other non-Ohmic nanopores.[22] Interestingly, the slope of the function $S(f)$ in a log−log representation was c with values between 1 and 2. In general, maltoporins and other bacterial outer-membrane proteins showed an ideal $1/f$ flicker noise function with $c \cong 1.0$.[5,12] However, deviations from the ideality of $1/f$ flicker noise have been determined in other cases.[15,18,69] It is not clear what the physical meaning of the departure of c from this ideality is. One possibility is that the low-frequency domain of the PSD is populated by a hybrid mixture of a $1/f$ noise factor and two or more Lorentzian distributions of white noise with different corner frequencies.[70,71] Here, this hypothesis is supported by the complex combination of a number of factors, such as the lack of $1/f$ noise from either Bs-released or Bs-captured substates, the dependence of $S(0)$ of the Bs-released substate on the Bs concentration, and the dependence of the frequency onset (f_{cut}) of the $1/f$ noise on the transmembrane potential.

https://dx.doi.org/10.1021/acs.langmuir.0c02498
Langmuir 2020, 36, 15247−15257

CONCLUSIONS

In this paper, we provide experimental evidence for the Bs-amplified $1/f$ noise of a protein-selective protein nanopore. Amplification in the low-frequency limit of current noise, $S(0)$, has been previously observed for ion channels permeating small-molecule analytes, such as protons,[27,28,31] sugars,[14,36] nucleotides,[64,72] and antibiotics.[73] Bn-t-FhuA also serves for explorations of reversible protein−protein interactions in real time and protein detection in an aqueous phase at single-molecule precision. Related protein nanopores have been previously developed by other groups using a diverse range of recognition elements, such as small molecules,[74−77] DNA aptamers,[78] and peptides.[30,79] The fundamental distinction of Bn-t-FhuA from other highly specific nanopores for protein detection is the relatively large size of the recognition element, which in this case is a 110-residue Bn protein.

In summary, we show significant qualitative and quantitative alterations in the low-frequency current noise regime of a protein-selective biological nanopore when a protein ligand is reversibly captured by its recognition element. This Bs-amplified $1/f$ noise is asymmetric with respect to the voltage bias and can be reverted back to a white-noise signature at Bs concentrations in excess. The reversible Bs-induced conductance switches appear to generate, at least in part, the $1/f$ noise in a Bs concentration-dependent fashion because the Bs-captured and Bs-released substates are virtually $1/f$ noise-free. It should be noted that these Bs−Bn binding interactions occur near the opening of the t-FhuA pore, so we conclude that the low-frequency $1/f$ flicker noise results from subtle Bs-induced alterations in the pore dynamics at the tip of the pore. Finally, this Bs-amplified low-frequency $1/f$ noise is likely generated by equilibrium conductance fluctuations because the low-frequency limit of the current noise, $S(0)$, is proportional to the square of applied transmembrane potential.[7,12,72]

ASSOCIATED CONTENT

Supporting Information

The Supporting Information is available free of charge at https://pubs.acs.org/doi/10.1021/acs.langmuir.0c02498.

Examples of single-channel electrical traces of Bn-t-FhuA at various Bs concentrations that were low-pass eight-pole Butterworth-filtered at 1 and 10 kHz; examples of single-channel electrical traces of Bn-t-FhuA at various applied transmembrane potentials that were low-pass eight-pole Butterworth-filtered at 10 kHz; PSDs of Bn-t-FhuA obtained at various applied transmembrane potentials; low-frequency limit, $S(0)$, of Bn-t-FhuA and its dependence on the squared transmembrane voltage and squared current; PSDs of Bn-t-FhuA in the presence of various Bs concentrations; PSDs of Bn-t-FhuA, which were normalized to the squared transmembrane current, in the presence of various Bs concentrations; examples of individual PSDs at various Bs concentrations; example of individual PSDs at various Bs concentrations, which resulted from the analysis of 20 s duration single-channel trace fragments; dependence of model-dependent and experimental low-frequency limits, $S(0)$, on the Bs concentration; PSDs of Bn-t-FhuA at various Bs concentrations but at a low positive potential; PSDs of Bn-t-FhuA obtained at high Bs concentrations; dependence of experimental and model-dependent low-frequency limit values, $S(0)$, on the Bs concentration in the high-concentration regime; PSDs of Bn-t-FhuA in the presence of a low-nanomolar Bs concentration and at various transmembrane potentials; and Johnson−Nyquist thermal noise and shot noise generated by the Bn-t-FhuA nanopore (PDF)

AUTHOR INFORMATION

Corresponding Author

Liviu Movileanu − *Department of Physics, Structural Biology, Biochemistry, and Biophysics Program, and Department of Biomedical and Chemical Engineering, Syracuse University, Syracuse, New York 13244-1130, United States;* orcid.org/0000-0002-2525-3341; Phone: 315-443-8078; Email: lmovilea@syr.edu; Fax: 315-443-9103

Authors

Jiaxin Sun − *Department of Physics, Syracuse University, Syracuse, New York 13244-1130, United States*

Avinash Kumar Thakur − *Department of Physics and Structural Biology, Biochemistry, and Biophysics Program, Syracuse University, Syracuse, New York 13244-1130, United States*

Complete contact information is available at: https://pubs.acs.org/10.1021/acs.langmuir.0c02498

Author Contributions

J.S. and A.K.T. contributed equally to this work. J.S., A.K.T., and L.M. designed research. J.S. and A.K.T. performed research and analyzed data. J.S., A.K.T., and L.M. wrote the paper.

Notes

The authors declare no competing financial interest.

ACKNOWLEDGMENTS

We are grateful to our colleagues in the Movileanu Laboratory for their comments and stimulating discussions as well as their assistance during the early stage of this project. We also thank Sergey Bezrukov for his insightful input regarding this article. This work was supported by the National Institute of General Medical Sciences of the U.S. National Institutes of Health, grants R01 GM088403 (to L.M.) and R01 GM129429 (to L.M.).

REFERENCES

(1) Noinaj, N.; Gumbart, J. C.; Buchanan, S. K. The β-barrel assembly machinery in motion. *Nat. Rev. Microbiol.* **2017**, *15*, 197−204.

(2) Slusky, J. S. Outer membrane protein design. *Curr. Opin. Struct. Biol.* **2017**, *45*, 45−52.

(3) Boyd, C. M.; Bubeck, D. Advances in cryoEM and its impact on β-pore forming proteins. *Curr. Opin. Struct. Biol.* **2018**, *52*, 41−49.

(4) Mondal, A. K.; Chattopadhyay, K. Taking Toll on Membranes: Curious Cases of Bacterial β-Barrel Pore-Forming Toxins. *Biochemistry* **2020**, *59*, 163−170.

(5) Wohnsland, F.; Benz, R. 1/f-Noise of open bacterial porin channels. *J. Membr. Biol.* **1997**, *158*, 77−85.

(6) Hooge, F. N.; Hoppenbrouwers, A. M. H. Amplitude distribution of 1/f noise. *Physica* **1969**, *42*, 331−339.

(7) Voss, R. F.; Clarke, J. Flicker (1f) noise: Equilibrium temperature and resistance fluctuations. *Phys. Rev. B: Solid State* **1976**, *13*, 556−573.

(8) Hooge, F. N. 1/f Noise. *Physica B+C* **1976**, *83*, 14−23.

(9) Orlik, F.; Schiffler, B.; Benz, R. Anthrax toxin protective antigen: inhibition of channel function by chloroquine and related compounds

and study of binding kinetics using the current noise analysis. *Biophys. J.* **2005**, *88*, 1715−1724.
(10) Fragasso, A.; Schmid, S.; Dekker, C. Comparing Current Noise in Biological and Solid-State Nanopores. *ACS Nano* **2020**, *14*, 1338−1349.
(11) Hilty, C.; Winterhalter, M. Facilitated substrate transport through membrane proteins. *Phys. Rev. Lett.* **2001**, *86*, 5624−5627.
(12) Bezrukov, S. M.; Winterhalter, M. Examining noise sources at the single-molecule level: 1/f noise of an open maltoporin channel. *Phys. Rev. Lett.* **2000**, *85*, 202−205.
(13) Andersen, C.; Cseh, R.; Schülein, K.; Benz, R. Study of sugar binding to the sucrose-specific ScrY channel of enteric bacteria using current noise analysis. *J. Membr. Biol.* **1998**, *164*, 263−274.
(14) Nekolla, S.; Andersen, C.; Benz, R. Noise analysis of ion current through the open and the sugar-induced closed state of the LamB channel of Escherichia coli outer membrane: evaluation of the sugar binding kinetics to the channel interior. *Biophys. J.* **1994**, *66*, 1388−1397.
(15) Siwy, Z.; Fulinski, A. Origin of 1/f(alpha) noise in membrane channel currents. *Phys. Rev. Lett.* **2002**, *89*, 158101.
(16) Banerjee, J.; Ghosh, S. Investigating interaction of ligands with voltage dependent anion channel through noise analyses. *Arch. Biochem. Biophys.* **2005**, *435*, 369−371.
(17) Tabard-Cossa, V.; Trivedi, D.; Wiggin, M.; Jetha, N. N.; Marziali, A. Noise analysis and reduction in solid-state nanopores. *Nanotechnology* **2007**, *18*, 305505.
(18) Smeets, R. M. M.; Keyser, U. F.; Dekker, N. H.; Dekker, C. Noise in solid-state nanopores. *Proc. Natl. Acad. Sci. U.S.A.* **2008**, *105*, 417−421.
(19) Smeets, R. M. M.; Dekker, N. H.; Dekker, C. Low-frequency noise in solid-state nanopores. *Nanotechnology* **2009**, *20*, 095501.
(20) Heerema, S. J.; Schneider, G. F.; Rozemuller, M.; Vicarelli, L.; Zandbergen, H. W.; Dekker, C. 1/f noise in graphene nanopores. *Nanotechnology* **2015**, *26*, 074001.
(21) Beamish, E.; Kwok, H.; Tabard-Cossa, V.; Godin, M. Precise control of the size and noise of solid-state nanopores using high electric fields. *Nanotechnology* **2012**, *23*, 405301.
(22) Powell, M. R.; Vlassiouk, I.; Martens, C.; Siwy, Z. S. Nonequilibrium 1/f noise in rectifying nanopores. *Phys. Rev. Lett.* **2009**, *103*, 248104.
(23) Hyland, B.; Siwy, Z. S.; Martens, C. C. Nanopore Current Oscillations: Nonlinear Dynamics on the Nanoscale. *J. Phys. Chem. Lett.* **2015**, *6*, 1800−1806.
(24) Hoogerheide, D. P.; Garaj, S.; Golovchenko, J. A. Probing surface charge fluctuations with solid-state nanopores. *Phys. Rev. Lett.* **2009**, *102*, 256804.
(25) Fragasso, A.; Pud, S.; Dekker, C. 1/f noise in solid-state nanopores is governed by access and surface regions. *Nanotechnology* **2019**, *30*, 395202.
(26) Tasserit, C.; Koutsioubas, A.; Lairez, D.; Zalczer, G.; Clochard, M. C. Pink noise of ionic conductance through single artificial nanopores revisited. *Phys. Rev. Lett.* **2010**, *105*, 260602.
(27) Bezrukov, S. M.; Kasianowicz, J. J. Current noise reveals protonation kinetics and number of ionizable sites in an open protein ion channel. *Phys. Rev. Lett.* **1993**, *70*, 2352−2355.
(28) Kasianowicz, J. J.; Bezrukov, S. M. Protonation dynamics of the alpha-toxin ion channel from spectral analysis of pH-dependent current fluctuations. *Biophys. J.* **1995**, *69*, 94−105.
(29) Bezrukov, S. M.; Krasilnikov, O. V.; Yuldasheva, L. N.; Berezhkovskii, A. M.; Rodrigues, C. G. Field-Dependent Effect of Crown Ether (18-Crown-6) on Ionic Conductance of α-Hemolysin Channels. *Biophys. J.* **2004**, *87*, 3162−3171.
(30) Harrington, L.; Cheley, S.; Alexander, L. T.; Knapp, S.; Bayley, H. Stochastic detection of Pim protein kinases reveals electrostatically enhanced association of a peptide substrate. *Proc. Natl. Acad. Sci. U.S.A.* **2013**, *110*, E4417−E4426.
(31) Nestorovich, E. M.; Rostovtseva, T. K.; Bezrukov, S. M. Residue ionization and ion transport through OmpF channels. *Biophys. J.* **2003**, *85*, 3718−3729.
(32) Danelon, C.; Nestorovich, E. M.; Winterhalter, M.; Ceccarelli, M.; Bezrukov, S. M. Interaction of zwitterionic penicillins with the OmpF channel facilitates their translocation. *Biophys. J.* **2006**, *90*, 1617−1627.
(33) Momben Abolfath, S.; Kolberg, M.; Karginov, V. A.; Leppla, S. H.; Nestorovich, E. M. Exploring the Nature of Cationic Blocker Recognition by the Anthrax Toxin Channel. *Biophys. J.* **2019**, *117*, 1751−1763.
(34) Yamini, G.; Nestorovich, E. M. Relevance of the alternate conductance states of anthrax toxin channel. *Proc. Natl. Acad. Sci. U.S.A.* **2017**, *114*, E2545−e2546.
(35) Kullman, L.; Winterhalter, M.; Bezrukov, S. M. Transport of maltodextrins through maltoporin: A single-channel study. *Biophys. J.* **2002**, *82*, 803−812.
(36) Andersen, C.; Jordy, M.; Benz, R. Evaluation of the rate constants of sugar–transport through maltoporin (LAMB) of escherichia-coli from the sugar-induced current noise. *J. Gen. Physiol.* **1995**, *105*, 385−401.
(37) Denker, K.; Orlik, F.; Schiffler, B.; Benz, R. Site-directed mutagenesis of the greasy slide aromatic residues within the LamB (maltoporin) channel of Escherichia coli: effect on ion and maltopentaose transport. *J. Mol. Biol.* **2005**, *352*, 534−550.
(38) Mohammad, M. M.; Howard, K. R.; Movileanu, L. Redesign of a Plugged β-Barrel Membrane Protein. *J. Biol. Chem.* **2011**, *286*, 8000−8013.
(39) Locher, K. P.; Rees, B.; Koebnik, R.; Mitschler, A.; Moulinier, L.; Rosenbusch, J. P.; Moras, D. Transmembrane signaling across the ligand-gated FhuA receptor: crystal structures of free and ferrichrome-bound states reveal allosteric changes. *Cell* **1998**, *95*, 771−778.
(40) Thakur, A. K.; Movileanu, L. Real-Time Measurement of Protein-Protein Interactions at Single-Molecule Resolution using a Biological Nanopore. *Nat. Biotechnol.* **2019**, *37*, 96−101.
(41) Schreiber, G.; Fersht, A. R. Interaction of barnase with its polypeptide inhibitor barstar studied by protein engineering. *Biochemistry* **1993**, *32*, 5145−5150.
(42) Deyev, S. M.; Waibel, R.; Lebedenko, E. N.; Schubiger, A. P.; Plückthun, A. Design of multivalent complexes using the barnase·barstar module. *Nat. Biotechnol.* **2003**, *21*, 1486−1492.
(43) Buckle, A. M.; Schreiber, G.; Fersht, A. R. Protein-protein recognition: Crystal structural analysis of a barnase-barstar complex at 2.0-.ANG. resolution. *Biochemistry* **1994**, *33*, 8878−8889.
(44) Thakur, A. K.; Movileanu, L. Single-Molecule Protein Detection in a Biofluid Using a Quantitative Nanopore Sensor. *ACS Sens.* **2019**, *4*, 2320−2326.
(45) Schreiber, G.; Fersht, A. R. Energetics of protein-protein interactions: Analysis ofthe Barnase-Barstar interface by single mutations and double mutant cycles. *J. Mol. Biol.* **1995**, *248*, 478−486.
(46) Guillet, V.; Lapthorn, A.; Hartley, R.; Mauguen, Y. Recognition between a bacterial ribonuclease, barnase, and its natural inhibitor, barstar. *Structure* **1993**, *1*, 165−176.
(47) Niedzwiecki, D. J.; Mohammad, M. M.; Movileanu, L. Inspection of the Engineered FhuA ΔC/Δ4L Protein Nanopore by Polymer Exclusion. *Biophys. J.* **2012**, *103*, 2115−2124.
(48) Thakur, A. K.; Larimi, M. G.; Gooden, K.; Movileanu, L. Aberrantly Large Single-Channel Conductance of Polyhistidine Arm-Containing Protein Nanopores. *Biochemistry* **2017**, *56*, 4895−4905.
(49) Wolfe, A. J.; Gugel, J. F.; Chen, M.; Movileanu, L. Kinetics of Membrane Protein-Detergent Interactions Depend on Protein Electrostatics. *J. Phys. Chem. B* **2018**, *122*, 9471−9481.
(50) Wolfe, A. J.; Gugel, J. F.; Chen, M.; Movileanu, L. Detergent Desorption of Membrane Proteins Exhibits Two Kinetic Phases. *J. Phys. Chem. Lett.* **2018**, *9*, 1913−1919.
(51) Couoh-Cardel, S.; Hsueh, Y. C.; Wilkens, S.; Movileanu, L. Yeast V-ATPase Proteolipid Ring Acts as a Large-conductance Transmembrane Protein Pore. *Sci. Rep.* **2016**, *6*, 24774.
(52) Larimi, M. G.; Mayse, L. A.; Movileanu, L. Interactions of a Polypeptide with a Protein Nanopore Under Crowding Conditions. *ACS Nano* **2019**, *13*, 4469−4477.

https://dx.doi.org/10.1021/acs.langmuir.0c02498
Langmuir 2020, 36, 15247−15257

(53) Bezrukov, S. M.; Liu, X.; Karginov, V. A.; Wein, A. N.; Leppla, S. H.; Popoff, M. R.; Barth, H.; Nestorovich, E. M. Interactions of high-affinity cationic blockers with the translocation pores of B. anthracis, C. botulinum, and C. perfringens binary toxins. *Biophys. J.* **2012**, *103*, 1208−1217.
(54) Kudlinzki, D.; Schmitt, A.; Christian, H.; Ficner, R. Structural analysis of the C-terminal domain of the spliceosomal helicase Prp22. *Biol. Chem.* **2012**, *393*, 1131−1140.
(55) Wolfe, A. J.; Si, W.; Zhang, Z.; Blanden, A. R.; Hsueh, Y.-C.; Gugel, J. F.; Pham, B.; Chen, M.; Loh, S. N.; Rozovsky, S.; Aksimentiev, A.; Movileanu, L. Quantification of membrane protein-detergent complex interactions. *J. Phys. Chem. B* **2017**, *121*, 10228−10241.
(56) Johnson, J. B. Thermal Agitation of Electricity in Conductors. *Phys. Rev.* **1928**, *32*, 97−109.
(57) Nyquist, H. Thermal agitation of electric charge in conductors. *Phys. Rev.* **1928**, *32*, 110−113.
(58) Sherman-Gold, R. Noise in Electrophysiological Measurements. *The Axon Guide*; Axon Instruments, Inc., 1993.
(59) Benndorf, K. Low-Noise Recording. In *Single-Channel Recoring*, 2nd ed.; Sakmann, B., Neher, E., Eds.; Plenum Press: New York, NY, 1995; pp 129−153.
(60) Uram, J. D.; Ke, K.; Mayer, M. Noise and bandwidth of current recordings from submicrometer pores and nanopores. *ACS Nano* **2008**, *2*, 857−872.
(61) Mayer, M.; Kriebel, J. K.; Tosteson, M. T.; Whitesides, G. M. Microfabricated teflon membranes for low-noise recordings of ion channels in planar lipid bilayers. *Biophys. J.* **2003**, *85*, 2684−2695.
(62) Palenskis, V.; Maknys, K. Nature of low-frequency noise in homogeneous semiconductors. *Sci. Rep.* **2015**, *5*, 18305.
(63) Rostovtseva, T. K.; Liu, T.-T.; Colombini, M.; Parsegian, V. A.; Bezrukov, S. M. Positive cooperativity without domains or subunits in a monomeric membrane channel. *Proc. Natl. Acad. Sci. U.S.A.* **2000**, *97*, 7819−7822.
(64) Rostovtseva, T. K.; Komarov, A.; Bezrukov, S. M.; Colombini, M. Dynamics of nucleotides in VDAC channels: structure-specific noise generation. *Biophys. J.* **2002**, *82*, 193−205.
(65) Hooge, F. N.; Kleinpenning, T. G. M.; Vandamme, L. K. J. Experimental studies on 1/f noise. *Rep. Prog. Phys.* **1981**, *44*, 479−532.
(66) Hooge, F. N. Discussion of recent experiments on 1/f noise. *Physica* **1972**, *60*, 130−144.
(67) Hooge, F. N. 1/f noise is no surface effect. *Phys. Lett. A* **1969**, *29*, 139−140.
(68) Mohammad, M. M.; Iyer, R.; Howard, K. R.; McPike, M. P.; Borer, P. N.; Movileanu, L. Engineering a Rigid Protein Tunnel for Biomolecular Detection. *J. Am. Chem. Soc.* **2012**, *134*, 9521−9531.
(69) Hooge, F. N. 1/f noise in the conductance of ions in aqueous solutions. *Phys. Lett. A* **1970**, *33*, 169−170.
(70) Sauvé, R.; Szabo, G. Interpretation of 1/f fluctuations in ion conducting membranes. *J. Theor. Biol.* **1985**, *113*, 501−516.
(71) Hooge, F. N.; Bobbert, P. A. On the correlation function of 1/f noise. *Physica B* **1997**, *239*, 223−230.
(72) Rostovtseva, T. K.; Bezrukov, S. M. ATP transport through a single mitochondrial channel, VDAC, studied by current fluctuation analysis. *Biophys. J.* **1998**, *74*, 2365−2373.
(73) Nestorovich, E. M.; Danelon, C.; Winterhalter, M.; Bezrukov, S. M. Designed to penetrate: Time-resolved interaction of single antibiotic molecules with bacterial pores. *Proc. Natl. Acad. Sci. U.S.A.* **2002**, *99*, 9789−9794.
(74) Movileanu, L.; Howorka, S.; Braha, O.; Bayley, H. Detecting protein analytes that modulate transmembrane movement of a polymer chain within a single protein pore. *Nat. Biotechnol.* **2000**, *18*, 1091−1095.
(75) Fahie, M. A.; Yang, B.; Mullis, M.; Holden, M. A.; Chen, M. Selective Detection of Protein Homologues in Serum Using an OmpG Nanopore. *Anal. Chem.* **2015**, *87*, 11143−11149.
(76) Fahie, M.; Chisholm, C.; Chen, M. Resolved single-molecule detection of individual species within a mixture of anti-biotin antibodies using an engineered monomeric nanopore. *ACS Nano* **2015**, *9*, 1089−1098.
(77) Fahie, M. A.; Chen, M. Electrostatic Interactions between OmpG Nanopore and Analyte Protein Surface Can Distinguish between Glycosylated Isoforms. *J. Phys. Chem. B* **2015**, *119*, 10198−10206.
(78) Rotem, D.; Jayasinghe, L.; Salichou, M.; Bayley, H. Protein Detection by Nanopores Equipped with Aptamers. *J. Am. Chem. Soc.* **2012**, *134*, 2781−2787.
(79) Harrington, L.; Alexander, L. T.; Knapp, S.; Bayley, H. Single-Molecule Protein Phosphorylation and Dephosphorylation by Nanopore Enzymology. *ACS Nano* **2018**, *13*, 633−641.

https://dx.doi.org/10.1021/acs.langmuir.0c02498
Langmuir 2020, 36, 15247−15257